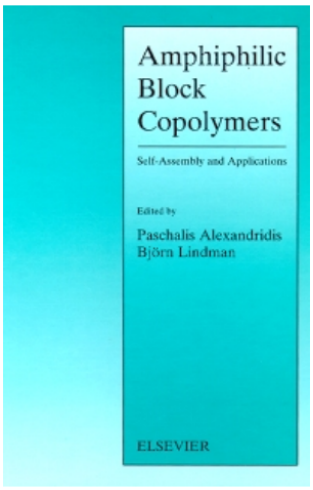

Amphiphilic Block Copolymers

1st Edition

Self-Assembly and Applications

☆☆☆☆☆ Write a review

Authors: P. Alexandridis, B. Lindman

Hardcover ISBN: 9780444824417
eBook ISBN: 9780080527109

Imprint: Elsevier Science
Published Date: 18th October 2000

Page Count: 448

View on ScienceDirect ↗

Google Preview

Author
P. Alexandridis
Department of Chemical Engineering, State University of New York at Buffalo, NY 14260-4200, USA
B. Lindman
Center for Chemistry and Chemical Engineering, S-22100 Lund, Sweden

Table of Contents

Details

Language:	English
Copyright:	© Elsevier Science
Published:	18th October 2000
Imprint:	Elsevier Science
Hardcover ISBN:	9780444824417
eBook ISBN:	9780080527109

Small-Angle Scattering Studies of Block Copolymer Micelles, Micellar Mesophases and Networks

Kell Mortensen[a]

[a]Condensed Matter Physics and Chemistry Department,
Risø National Laboratory, DK-4000 Roskilde, Denmark.

Small-angle scattering is a key technique in relation to experimental studies of complex fluids and polymers. The application of small-angle neutron scattering is reviewed in relation to structural studies of block copolymers and their solutions. It is shown that such scattering experiments provide detailed information on both size and form of the polymer as well as their aggregates, and on the thermodynamics characterizing the self-assembling. The scattering data gives the detailed structure of block copolymer micelles as well as information on the inter-micellar interactions. In dense systems, the small-angle technique is used to study thermodynamics of the disorder-to-order phase transitions, and to study details of the ordered phases. It is shown that aqueous systems of triblock copolymers composed of poly(ethylene oxide) and poly(propylene oxide) have not only interests for applications, but constitute a very good model system in which a variety of thermodynamics can be studied. This include for example the unimer-to-micelle self-assembling, micellar sphere-to-rod shape transformation, micellar hard-sphere crystallization into cubic or hexagonal order, and order-to-bicontinuous phase-transitions.

1. INTRODUCTION

Static and dynamic neutron scattering have been key techniques in studying the basic properties and revealing some of the universal structures and scaling laws for polymers and other complex fluids.

An important property of complex polymer materials is the degree of miscibility between various units in the material, i.e. the miscibility between polymers and a solvent, between different polymers, or between various regimes (blocks) within a single polymer chain. This factor plays a main role for the material properties and phase behavior. As a general rule it is found that polymers do not mix. When low-molecular weight liquids normally makes an ideal mixture, this is a result of the dominating entropic contribution to the Gibbs free energy. Even though the intermolecular forces usually are repulsive, the enthalpic contribution is only small (except for special liquids like water). In polymers, on the other hand, the gain in mixing-entropy is very much reduced due to the large molecular dimensions, whereas the enthalpic parts remain like small molecules. Therefore, it is practically only possibly to make ideal blends of few, special polymers.

The absence of miscibility is, on the other hand, the basis for attractive structural properties. When various parts within a single chain are immiscible, or have different sol-

ubility in selective solvents, the molecules may self-assembly into well organized structures to minimize direct contact between the immiscible units. This self-association gives rise to a wide range of phase behavior, including the formation of micelles of various form and sizes, complex structured microemulsions, and liquid crystalline phases on the mesoscopic length scale.

The association of amphiphilic macromolecules into complex structures is analogous to that of small surfactants like soaps and lipids. The polymeric nature of amphiphil macromolecules will, however, give rise to new properties which may be the basis for important extensions of the use of amphiphil molecules.

Diblock and triblock copolymers have been extensively studied both in the melt and in solution. The solutions, which is the main topic of here, are in particular interesting when only one of the blocks are soluble. In such case a variety of aggregates may be formed, depending on the molecular architecture. Often, the polymers then self-associate into microscopic well defined aggregates where the non-soluble parts form a core shielded from the solution by the soluble blocks. Such micellar aggregates may have the form of spherical objects, or they may be elongated stif rods or less flexible 'worms', or have the form of flat discs. More complex structures can also be found, as for example networks of micelles or bi-continuous phases.

A variety of block copolymers have been investigated when mixed with a selective solvent. These include organic solvents with copolymers composed of blocks of poly(styrene), PS; poly(isoprene), PI; poly(ethylene), PE; poly(ethylene propylene), PEP; and poly(ethylene butylene), PEB. Most of the polymers which have been studied in relation to aqueous solutions, are based on poly(ethylene oxide), PEO, as the water soluble block. The non- or less-soluble blocks have f.ex. been poly(propylene oxide), PPO [1–4], poly(dimethyl siloxane) (PDMS) [5] poly(butylene oxide), PBO [6], poly(styrene) [7], and poly(isobutylene), PIB [8]. Most experimental as well as applied studies have concerned triblock copolymers with the center block of poly(propylene oxide), PPO, known as Pluronics or Poloxamers. A large number of papers on such PEO-PPO-PEO tri-block copolymers have been published in the last few years, including extended reviews [1–4]. Only few studies have been published on the reversed Pluronics with molecular architecture PPO-PEO-PPO [9]. The PEO-PPO block copolymers constitute an ideal model system to study the properties as a function of amphiphil character. While PEO is water soluble within the 0-100°C-temperature range, PPO is only soluble at low temperatures and for relative low polymer concentrations. It is therefore possibly to control the degree of the amphiphil character of the block-copolymer, just by varying the temperature.

Below we will focus on di- and tri-block copolymers which self-organize into micellar aggregates. We will discuss both AB, ABA and BAB type of chemical architecture, where A is the soluble block. The AB and ABA type of systems to be discussed organize as a general rule in individual micellar aggregates, which interact through a near hard-sphere type of potential. Such micellar systems are visualized in Fig. 1. BAB polymers may also form individual micelles, but this imply that all polymer chains start and end in the same micelle having the middle A-block dispersed into the liquid. More likely, such micelles form interconnected networks, where cores are connected by the soluble A-polymer block, as shown schematically in Fig. 2.

Scattering experiments give important insight into the assembling characteristics. Fig. 3

and Fig. 4 shows the characteristic scattering pattern, $I(q)$, typically obtained from aggregates of respectively AB(A) and BAB type of block copolymers. The peak is indicative of interacting micelles. The peak position depends on both the (local) micellar volume fraction and the interaction distance.

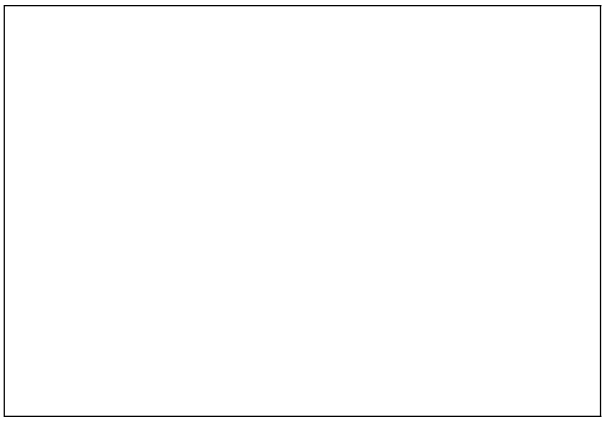

Figure 1. Schematic representation of spherical micelles of AB and/or ABA type of block copolymers in A-solvent, resulting in independent hard-sphere interacting spherical aggregates.

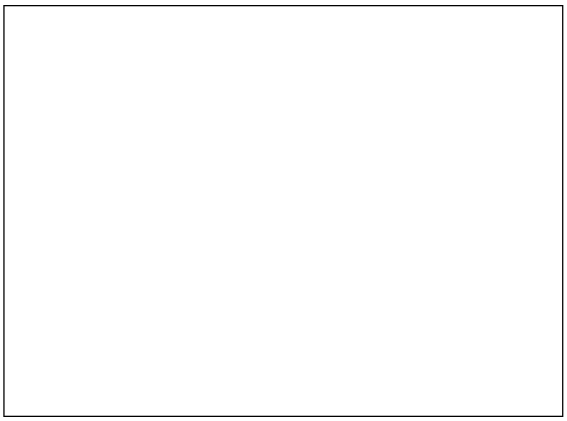

Figure 2. Schematic representation of spherical micelles of BAB type of block copolymers in A-solvent, resulting in domains of interconnected networks of spherical aggregates.

Block copolymer micellar aggregates have wide range of potential and applied uses, as for example viscosity controlling agents, soaps and detergents, lubricant's and units for controlled drug release. An important class of block copolymers are those in which water is a selective solvent.

2. Small Angle Scattering Instrumentation

Small-angle x-ray (SAXS) and neutron scattering (SANS) facilities consists in principle of few, independent units: the radiation source, the monochromating system, the collimator and the detector. In addition, special sample environment are typically an integrated part of the instrument. While most SAXS instruments are laboratory facilities, SANS facilities must due to the need for intense neutron flux always be located at large installations of either thermal research reactors or neutron-spallation sources. The additional possibilities for high resolution and quick data sampling from synchrotron x-ray sources, do, however, make the use of such SAXS-instruments at large installations still more important.

2.1. Small-Angle X-ray Scattering

In instruments using conventional x-ray tubes as the source, the Kratky type of SAXS instrument is the most commonly used [10]. This type of instrument has optimized the

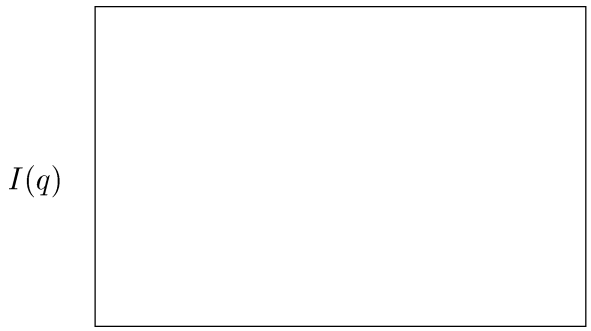

Figure 3. Typical scattering function of individual, hard-sphere interacting micelles.

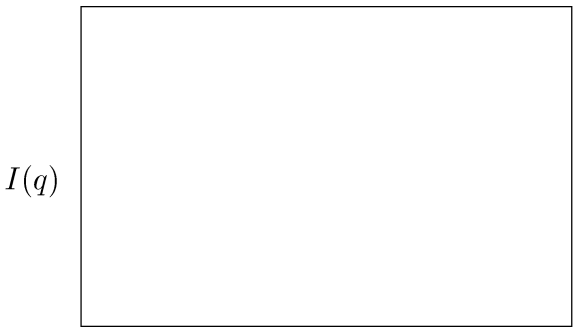

Figure 4. Typical scattering function of networks of connected spherical micelles.

flux and resolution using slit geometry for collimation and simple filter for monochromatization. The detector is a simple or a linear sensitive detector. The Kratky-apparatus is often sufficient for studies of solution with not too anisotropic aggregates. The Kratky instrument has also successfully been used in studies of micelles with liquid crystalline order [11], but due to the extreme anisotropic resolution function it may cause significant problems in such samples, with misleading values of scattering momenta. In x-ray sources of high power rotating anodes and synchrotron facilities, pin-hole cameras are usually used. In these systems the collimation consists of two pinhole to define the beam, one near the source, and a second relative near the sample. A third pinhole is usually needed between the defining pinhole and the sample to reduce parasitic scattering and Fraunhofer diffraction from the slits. The monochromatization is obtained using Bragg-scattering from single crystals, and the scattered photon are detected by an area sensitive detector.

2.2. Small-Angle Neutron Scattering

Small-angle neutron scattering instruments are basically always of the pin-hole type, and facilitated with area sensitive detectors. In thermal reactor instruments, the monochromatization is usually obtained using the transmission of a mechanical velocity selector. Few instruments uses the Bragg scattering from a crystal with broad mosaic spread, or super mirrors. Spallation source instruments can also with advance use such monochromatization units, in particular in the case of significant inelastic scattering processes. Usually, however, the full beam is used, and time of flight analysis split the spectra into given neutron wavelengths.

2.3. Auxcilliary in situ devices.

The success of many recent studies utilizing small-angle scattering technique for polymers and liquids, are facilitated by the access to new experimental tools which can be operated *in situ* during the scattering experiment. These include pressure cells [12] and mechanical stretching and shearing devices [13]. Within studies of soft condensed matter the application of shear field has in particular given important new insight into the under-

lying physics. Hadziioannou et al. [14] showed that highly oriented cylinder and lamellae structures of block copolymer melts could be produced in oscillatory shear flow, whereas Bates and coworkers demonstrated shear oriented single domain cubic phases [15,16]. Ackerson et al. [17] and Lindner et. al. [18], have shown how colloidal crystals can be oriented in the continuous shear flow in a Couette cell. Block copolymer micellar crystals can equivalently be oriented in the Couette cell, as shown by Mortensen et al. [19] and Gast et al. [20].

2.4. Couette shear cell

A simple shear cell used in SANS experiments is the Couette type shown schematically in Fig. 5. Both inner and outer cylinders of the Couette cell can be manufactured of neutron transparent materials like quartz, aluminium or niobium. In the design of Fig. 5 the apparatus is contained in a larger steel cylinder allowing removal of the driving motor and inner Couette cylinder from the top through the open shaft. Conical contact surfaces guarantee that the inner cylinder always is in perfect centricity with the outer cylinder. The outer cylinder is mounted vacuum tight to the bottom of the steel cylinder with a 120° V-shaped inside bottom to prevent air bubbles being caught when the cell is spun. The diameter of the inner cylinder is typically of the order of 30 mm, and the annular gap of 0.5-1 mm. The apparatus is placed in the horizontal neutron beam so that the neutrons pass either radially through the center of the cylinders, or tangential to the cylinder. Couette devices are typically operated with shear gradients in the $\dot{\gamma}$=1−3000 $\sec^{-1}$ range.

Figure 5. Sketch of Couette cell for SANS.

Figure 6. Sketch of parallel plate shear device for SANS.

2.5. Parallel Plate Cell

A parallel-plate device for *in situ* studies of block copolymer melts and more viscous micellar suspensions are shown schematically in Fig. 6. The fist instrument of this type

were specially constructed for SANS [13,21], while more recent devises for both neutrons (Risø) and x-ray (Daresbury) facilities have modified a commercial rheology instrument (Rheometrics, RSA2), thus providing the possibility for simultaneous rheological and structural information.

2.6. Pressure Cell

Pressure cells for studies of complex liquids exists for both x-ray and neutrons. The typical range of available pressures are in the 1-2000 bar range.

3. Scattering function from dilute solutions.

The theory of small-angle scattering has been presented in various text books [10,22–24] and will only briefly be reviewed below.

The interaction between matter and radiation is for x-ray scattering dominated by the response of the electrons which is accelerated in the electric field of the beam. To a good approximation each electron scatters the beam as a dipole proportional to the term $b_e = e^2/m_e c^2$, where e is the electronic charge, m_e the electron mass and c the velocity of light. b_e, which has the dimension of length, b_e=0.282·10^{-4}Å, is the 'scattering length'. In the interaction with an atom, one must integrate over all electrons, taking the phases into account:

$$b_z = \int b_e \rho(r) d^3 r \tag{1}$$

where $\rho(r)$ is the charge distribution in the atom. The integral, which depends on the scattering angle θ, defines the *atomic form factor*. For small-angle scattering ($\theta \approx 0$), the $\int \rho(r) d^3 r$-term approaches the number of electrons, i.e. Z, thus giving the atomic scattering length $b_Z \approx b_e Z$.

The interaction between neutrons and (non-magnetic) matter is dominated by the interaction with the nuclei. The scattering from different isotopes of the same atom may therefore be quite different. This is in particular the case for the two hydrogen isotopes, ^{1}H (abbreviated H) and ^{2}H (abbreviated D for deuterium). Since the neutron is a spin-$\frac{1}{2}$ particle there are two different couplings between the neutrons in the beam and a nucleous, unless the nucleous spin approach null (as in for example ^{16}O and ^{12}C, see Table 1). The average of these two interactions gives coherent scattering, whereas the deviation from average is incoherent and gives a uniform background. Only the coherent scattering term give information on the static structure. In Table 1 is given the scattering lengths of the most relevant atoms for polymer solutions.

The amplitude of x-ray or neutron radiation scattered from a collection of objects, located by vectors $\bar{r}_i$ and characterized by the scattering length b_i is given by

$$f(q) = \sum b_i \cdot \exp[i(\bar{q} \cdot \bar{r}_i)] \tag{2}$$

where $\bar{q}$ is the momentum transfer with length $|\bar{q}| = q = 4\pi/\lambda \sin(\theta/2)$, λ being the radiation wavelength and θ being the scattering angle. The intensity $I(q)$ is proportional to the square of the scattering amplitude

$$I(q) = K \cdot |f(q)|^2 \tag{3}$$

Table 1
Neutron scattering parameters

Nuclei	Coherent Scattering Length	Incoherent Scattering Length
^{1}H	-0.374 $\cdot 10^{-12}$cm	2.527 $\cdot 10^{-12}$cm
^{2}H	0.667 $\cdot 10^{-12}$cm	0.404 $\cdot 10^{-12}$cm
^{16}O	0.580 $\cdot 10^{-12}$cm	0.0 $\cdot 10^{-12}$cm
^{12}C	0.665 $\cdot 10^{-12}$cm	0.0 $\cdot 10^{-12}$cm
^{14}N	0.937 $\cdot 10^{-12}$cm	0.20 $\cdot 10^{-12}$cm
^{28}Si	0.411 $\cdot 10^{-12}$cm	0.0 $\cdot 10^{-12}$cm
^{31}P	0.513 $\cdot 10^{-12}$cm	0.02 $\cdot 10^{-12}$cm
^{35}Cl	1.165 $\cdot 10^{-12}$cm	0.61 $\cdot 10^{-12}$cm

Ref: Neutron News, Vol 3, 1992

where K is given by the geometrical configuration, the intensity of the incident flux, and the sample transmission. Normalizing with respect to these parameters, we get the differential cross section $d\sigma/d\Omega$. From Eq. 2, $d\sigma/d\Omega$ can thus be written

$$\frac{d\sigma(q)}{d\Omega} = \sum\sum b_i b_j \exp[i(\bar{q}\cdot\bar{r}_{ij})] \tag{4}$$

where $\bar{r}_{ij} = \bar{r}_i - \bar{r}_j$. It is useful to replace the scattering length b with the parameter η describing fluctuations from average: $\eta = b - < b >$, and defining the correlation function $\gamma_{ij} = \eta_i\eta_j / < \eta^2 >$. Inserted in Eq. 4, this gives

$$\frac{d\sigma(\bar{q})}{d\Omega} =< \eta^2 > \cdot \sum \gamma_{ij} \exp[i(\bar{q}\cdot\bar{r}_{ij})] \tag{5}$$

In small-angle scattering experiments the resolution is not on atomic distances ($\sim$ 1Å). The scattering lengths may therefore be replaced by a continuous function, defined as the scattering length density, ρ, given by $\rho = \sum b_i/V$, where V is an appropriate (molecular) volume. Equivalently, the fluctuation parameter η is redefined as a continuous function: $\eta(\bar{r}) = \rho(\bar{r}) - < \rho >$. The prefactor $< \eta^2 >$ is in a two-component system with scattering length density ρ_1 and ρ_2 easily shown to be equal $(\rho_1 - \rho_2)^2 = \Delta\rho^2$. With the summation in Eq. 5 replaced by an integration, we then have:

$$\frac{d\sigma(\bar{q})}{d\Omega} = \Delta\rho^2 \int_{sample} \gamma(\bar{r}) \exp[i(\bar{q}\cdot\bar{r})] d\bar{r} \tag{6}$$

The integration in Eq. 6 is over the whole sample volume. For a monodisperse ensemble of scattering objects, particles, the integration of the correlation function can be split into the intra-particle self-correlation term and the inter-particle correlation giving

$$\frac{d\sigma(\bar{q})}{d\Omega} = nV^2(\Delta\rho)^2 \cdot \int_{intra} \gamma(\bar{r}) \exp[i(\bar{q}\cdot\bar{r})] d\bar{r} \cdot \int_{inter} (\gamma(\bar{r}) - 1) \exp[i(\bar{q}\cdot\bar{r})] d\bar{r} \tag{7}$$

where n is the number density of particles, and spherical symmetry is assumed. The first integral in Eq. 7 determines the normalized particle form factor, $P(q)$, and the last

integration term gives the inter-particle structure factor, $S(q)$. The scattering function can thus be written

$$\frac{d\sigma(\bar{q})}{d\Omega} = n\Delta\rho^2 V^2 P(q) S(q) \tag{8}$$

For very dilute systems, $S(q)$=1 and the particle form factor is determined directly from the scattering function.

For polydisperse systems Pedersen [25] proposed an approximation assuming sub-systems of monodisperse ensembles. The total scattering function is then the sum of these systems weighted by a size distribution function $D(R)$

$$\frac{d\sigma(\bar{q})}{d\Omega} = \Delta\rho^2 \int D(R) V^2(R) P(q) S(q) dR \tag{9}$$

Kotlarchyk and Chen [26] showed that it is possibly formally to write the scattering function of polydisperse systems as Eq. 8, but with the form factor replaced by the weighted mean value:

$$V^2 \tilde{P}(q) =< V^2 P(q) >$$

and the structure factor replaced with

$$\tilde{S}(q) - 1 = \beta(q)[S(q) - 1],$$

where $\beta(q)$ is a correction term determined by the degree of polydispersity. The scattering function of non spherical particles can be treated equivalently, using Eq. 8.

3.1. Contrast Variation

Small-angle neutron scattering experiments are particularly useful for detailed studies of the local structures of block copolymer aggregates. This is done by systematic studies of systems in which the contrast is varied by exchanging hydrogens with deuterium in specific places. This is most easily done simply by changing the composition of the solvent in terms of normal and deuterated material. Alternatively, specific deuterium labeling is chemically build into the block copolymer molecule during the synthesis. While the effect of changing the contrast of a pure two-phase systems is only to change the prefactor in front of the scattering function, more complex structures with varying scattering length density gives significant different form of the scattering function. This is shown in the example given in Fig. 7, showing PEO-PPO-PEO micelles in mixtures of water and oil, with different contrasts.

4. Model Functions

In the following we will assume that the block copolymer aggregates are monodisperse and randomly oriented, so Eq. 8 is valid. We will review some of the most important analytical expressions for the scattering function of typical block copolymer aggregates, eg. micelles with spherical, elliptical or rod-like shapes. Most of the expressions can be found in the book of Guinier and Fournet [22], or in the extended list of known scattering cross sections recently summarized by Pedersen [28].

Figure 7. Scattering function of PEO-PPO-PEO block copolymer aggregate in mixture of water and oil, with two different contrasts [27].

4.1. Block Copolymers Dissolved as Gaussian Coils

If the solvent is a theta solvent for both blocks, the copolymers will be dissolved as individual random coils. The scattering function is then determined by the Debye function, F_c [22]:

$$F_c(q) \sim x^{-2}(\exp(-x) + x - 1) \tag{10}$$

where $x{=}(qR_g)^2$, R_g being the polymer radius of gyration.

4.2. Scattering from Spherical Micelles

The form factor, F_s of a homogeneous spherical particle with radius R_c has the analytical form [22]

$$F_s(q) = [\Phi_s(q)]^2 = [\frac{3}{(qR_c)^3}(\sin(qR_c) - qR_c\cos(qR_c))]^2 \tag{11}$$

which approach the $F_s(q) \propto q^{-4}$ Porod law at large q-values.

The form factor Eq. 11 represents a good approximation to block copolymer micelles if they form a dense spherical aggregate, or if the contrast of the micellar corona has been matched to the solvent. The spectrum shown in Fig. 7 represents the latter situation.

Typically, however, the micelles are of the 'star-type' (Fig. 1) with relative dense cores of the non-soluble blocks and a corona of the soluble part extended into the solvent. At large q-values such block copolymer micelles rather shows a form factor which approach a q^{-2} behavior at large q-values.

4.2.1. Concentric Spherical Shells

A possibly solution for better description of such spherical symmetric micelles is to use the form factor of concentric shells.

The form factor of a single shell with inner and outer radius R_1 and R_2, respectively, is obtained from the form factor of dense sphere, $P = P_{sphere}$ (Eq. 11) by subtracting the empty core with the proper volume weighting [22]:

$$P(q) = \frac{V(R_1)P_{sphere}(q, R_1) - V(R_2)P_{sphere}(q, R_2)}{V(R_1) - V(R_2)} \tag{12}$$

This form factor can be generalized to a form factor of N concentric shells with radii R_i and ρ_i being their respective scattering length densities:

$$P(q) = \frac{\rho_1 V(R_1)P_{sphere}(q, R_1) + \sum(\rho_i - \rho_{i-1}V(R_i)P_{sphere}(q, R_i)}{\rho_1 V(R_1) + \sum V(R_i)(\rho_i - \rho_{i-1}} \tag{13}$$

4.2.2. Micellar Form Factor

A more realistic form factor of spherical block-copolymer micelles including the dense core and corona of Gaussian chains can be approached by an analytical expression [29]. This form factor includes both the self-correlation of the spherical core, self-correlation of the chains in the corona, the cross term between the core and chains and cross term between different chains. The self-correlation term of the sphere (F_s and Φ_s) and chains (F_c) are given by the formula Eq. 11 and Eq. 10, respectively. The cross terms are calculated using the Debye equation, using infinitely thin shells and taken into account the correct weighting functions for, respectively, solid sphere and Gaussian chains. The interference term between core and chains thereby get the form:

$$S_{sc}(q) = \Phi_s(q, R_c)x^{-1}(1 - e^{-x})\sin(qR_c)/(qR_c) \tag{14}$$

and the term between chains attached to the surface:

$$S_{cc}(q) = x^{-2}(1 - e^{-x})^2\ [sin(qR_c)/(qR_c)]^2 \tag{15}$$

where x=$(R_g q)^2$, as before. The resulting form factor of a block-copolymer micelle with aggregation number N_{agg} can then be expressed as [29]

$$F_{mic}(q) = N_{agg}^2\rho_s^2 F_s(q, R)+N_{agg}\rho_c^2 F_c(q, L, b)+N_{agg}(N_{agg}-1)\rho_c^2 S_{cc}(q)+2N_{agg}\rho_s\rho_c S_{sc}(q) \tag{16}$$

where ρ_s and ρ_c are the excess scattering length densities of blocks in the core and in the chains of the corona, respectively.

4.3. Ellipsoidal Micelle

The form factor of a dense ellipsoid with rotation symmetry is not analytically, but must be calculated numerically. Averaging over orientations gives the form factor for an ellipsoid with axes R, R, ϵR [22]

$$P(q) = \int_0^{\pi/2} [\frac{3(\sin(qR) - qR\cos(qR)}{(qR)^3}]\ \sin\alpha\ d\alpha \tag{17}$$

The form factor for concentric ellipsoidal shells can be calculated in analogy to that of concentric spheres.

4.4. Rod-Like Micelles

The form factor expression for rod-like micelles involves an integration over the first order Bessel function $B_1(x)$. The form factor of rods with radius R and length L has the form [22]

$$P(q) = \int_0^{\pi/2} [\frac{2B_1(qR\sin\alpha)}{qR\sin\alpha} \cdot \frac{\sin(qL\cos\alpha)/2}{qL\cos\alpha/2)}]^2 \cdot \sin\alpha \; d\alpha \tag{18}$$

4.5. Inter-Micellar Correlations

The scattering function of micellar solutions, Eq. 8, becomes increasingly dominated by the structure factor $S(q)$ as the micellar concentration is increased.

The structure factor can often successfully be determined using the Ornstein-Zernike and Percus-Yevick approximations [30] using a hard-sphere interaction potential, but other approximations are also available. $S(q)$ is in the hard-sphere Percus-Yevick approximation given by the micellar volume fraction ϕ and the hard-sphere interaction distance R_{hs} [31–33]:

$$S(q) = \frac{1}{1 + 24\phi G(qR_{hs}, \phi)/(2qR_{hs})} \tag{19}$$

where G is a trigonometric function of $y{=}qR_{hs}$ and ϕ

$$\begin{aligned} G(y,\phi) \;\; = \;\; & \alpha(\phi)/4y^2 \cdot [\sin(2y) - 2y\ \cos(2y)] + \beta(\phi)/8y^3 \cdot [4y\ \sin(2y) + (2-4y^2)\cos(2y) - 2] \\ & + \gamma(\phi)/32y^5 \cdot [-16y^4\ \cos(2y) + 4[(8y^2-6)\cos(2y) + (8y^3-12y)\sin(2y) + 6]] \end{aligned}$$

and α, β, and γ are given by the hard sphere volume fraction ϕ:

$$\begin{aligned} \alpha &= (1+2\phi)^2/(1-\phi)^4 \\ \beta &= -6\phi \cdot (1+\phi/2)^2/(1-\phi)^4 \\ \gamma &= \phi/2 \cdot (1+2\phi)^2/(1-\phi)^4 \end{aligned}$$

The peak-position q_{max} of $I(q)$ of hard-sphere systems are frequently interpreted simple as given by the mean micellar distance: $2\pi/q_{max} = D = [\frac{4\pi}{3}R_{hs}^3/\phi]^{1/3}$, i.e. given by the micellar number density only. This is not true, the position of q_{max} is determined by a complex function of R_{hs} and ϕ.

5. Examples:

Aqueous solutions of block copolymers of PEO and PPO constitutes an ideal class of systems in which self assembling and correlations can be studied in great details. The solubility of PPO in water changes markedly by relative small changes in thermodynamic parameters like temperature and pressure. It is therefore possibly in details to study phenomena like the micelle-formation as a function of the amphiphilic character of the molecules continuously by for example changing the temperature. Likewise, it is possibly to study form-transformations of the aggregates, as well as correlations between aggregates and possibly crystalline mesophases. Below, we will show examples of the use of small angle scattering technique for studies of micellar systems. The examples will mainly be taken from studies of Pluronics, but some other systems are mentioned as well.

5.1. Unimers

The miscibility of polymers in solvents may vary substantially with polymer concentration and thermodynamic parameters like temperature and pressure. This is for example the situation for poly(propylene oxide), PPO, in water. PPO is soluble in water only at low temperatures and relative low polymer concentrations. Block copolymers of water soluble poly(ethylene oxide), PEO, and PPO therefore appear as independent polymer chains, called *unimers*. Within statistical error, the scattering function of these unimers is in agreement with the polymers obeying Gaussian conformation. This is shown by the experimental scattering data of 5% $EO_{99}PO_{65}EO_{99}$ (F127) obtained at T=5°C, given in Fig. 8. The solid line represents the best fit to the Debye function of Gaussian chains, Eq. 10, including instrumental smearing and a constant I_{ic} which represents incoherent background from the sample. The resulting radius of gyration for $EO_{99}PO_{65}EO_{99}$ is R_g=22Å. Equivalent good agreements to the Debye function have within statistical error been observed in other Pluronics [33–35].

Figure 8. Scattering function of an aqueous solution of $EO_{99}PO_{65}EO_{99}$ unimers (5% solution at 5°C). The solid line represents the best fit to the Debye-function.

Figure 9. The radius of gyration R_g as obtained from SANS data of a variety of PEO-PPO-PEO unimers in aqueous solutions. The dotted line represents the expected R_g-values expected for Gaussian conformation with monomer size 2Å and Kuhn segment length 10Å.

Fig. 9 shows the experimental R_g values of different Pluronics, as plotted against the total number of monomers ($2m$+n). The experimental R_g values appear rather small if the copolymers really are dissolved as Gaussian chains. It has been argued that acqueous solution of PEO-chains with more than 10 units are predominantly in the helical meander configuration [36,37] with monomer length l of the order of 2Å. The Kuhn segment length b is of the order of 10Å [38,29]. If we assume that the PPO chain have the same characteristics as the PEO chain (which is a lower limit) this leads to a radius of gyration

R_g=$\sqrt{Nlb/6}$=30Å for $EO_{99}PO_{65}EO_{99}$. The broken line in Fig. 4 represents this calculation as a function of N=$2m$+n. The reduced experimental value of R_g may indicate that the less soluble PPO-block is significant more compact than Gaussian chain. The unimer thus resemble that of a uni-molecular micelle.

5.2. Spherical Micelles

The poly(propylene oxide) block becomes more hydrophobic upon increasing temperature. For a wide range of Pluronics, this leads to a well defined temperature upon which spherical micelles are formed. These micelles are composed of a core dominated by propylene oxide blocks, and surrounded by a corona of hydrated ethylene oxide subchains. Model calculation have been able to describe adequately the micellation process and proved that the PPO blocks are responsible for the entropy-driven micellation process [39,40].

The scattering function of $EO_{99}PO_{65}EO_{99}$-micelles in a 1%, 2% and 5% polymer solutions are shown in Fig. 10 [41]. The data have been normalized to polymer concentration. The scattering functions clearly show a side maximum as expected from the formfactor of dense spherical objects with sharp interface

Figure 10. Experimental scattering function of $EO_{99}PO_{65}EO_{99}$-micelles in a 1%, 2% and 5% aqueous solutions. The data have been normalized to polymer concentration. The solid line represents best fits to the micellar scattering function, Eq. 16, including hard-sphere inter-micellar correlations, Eq. 19.

It appear from Fig. 10 that the position of the side maximum is effectively unaffected by the polymer concentrations, showing that the micellar size, and thereby the aggregation number, is rather independent of the polymer concentration. At low q-values, on the other hand, a significant reduction in scattering intensity is seen resulting from inter-micellar correlations of higher concentrations. The temperature dependence (not shown) of the side-maxima is also weak, but significant, reflecting an increase in micellar size upon raising temperatures.

The significance of the side maximum is different for different Pluronics. For low molecular weight systems, the side maximum is significantly reduced, if visible at all. The side-maximum observed in neutron scattering of Pluronic micelles is generally weak due

to the rather gradual change in scattering length density at the interface between the micellar core and corona. Since there is quite some difference in electron density from the PPO-melt core to the hydrated PEO corona, x-ray scattering has a larger change in scattering length density. x-ray scattering shows accordingly significantly more pronounced side maxima[42]. The factor which reduces the side-maxima in both x-ray and neutron scattering experiments, is possibly dispersity in size or shape. It thus seems that the high-molecular weight Pluronic micelles have significantly more well characterized spherical shape and size than low molecular systems.

Excellent fits are obtained to the experimental scattering function as represented by the representative $EO_{99}PO_{65}EO_{99}$ micellar data shown in Fig. 10. The solid lines are best fit using Eq. 16, and including instrumental smearing.

In the attempt to reduce the number of fitting parameters when analyzing extended number of scattering data, one may simple use the formfactor of dense spheres (Eq. 11) rather than the more complex (Eq. 16). Good fits are then obtained to the experimental scattering function for q-values up to approximately 2-3 times the peak-position $q_\circ$. The scattering function is thereby expressed in an analytical form determined by only three parameters: the hard-sphere volume fraction ϕ, and the two radii characterizing the micelles: the core-radius R_c and the hard-sphere interaction radius R_{hs}. In extended data sets one can then obtain detailed information on the temperature and concentration dependence of the micellar structure.

It is important to note, that in spite of the dispersed polymer corona a near-hard sphere interaction potential is expected as a result of entropic repulsion.

5.2.1. Micellar Size and Aggregation Number

As already concluded based on the position of the side maximum observed in the formfactor, the Pluronic micellar core-radius, R_c, appear to be basically independent of polymer concentration (Fig. 10). Likewise the hard-sphere interaction radius is relative independent of concentration, showing that the thermodynamics controlling the copolymer aggregation first of all is determined by temperature.

An increase in both R_c and R_{hs} of the PEO-PPO-PEO micelles upon increasing temperatures reflects changes in aggregation number. The core radius of $EO_{25}PO_{40}EO_{25}$ micelles, as an example, changes from approximately 40Å at 20°C to 50Å at 50°C. Simultaneously, the hard-sphere interaction radius changes from 50 to 70Å. The changes in the micellar sizes with temperature show that the micelles are dynamic aggregates in which the individual copolymer chains constantly move from one micelle to another. This allows optimizing the aggregation number according to thermodynamic parameters.

The change in micellar radius for different Pluronics shows very similar characteristics. Fig. 11 shows in a double logarithmic plot R_c versus reduced temperature for the series of PEO-PPO-PEO micelles with similar size PPO block: $EO_{25}PO_{40}EO_{25}$, $EO_{65}EO_{39}EO_{65}$ and $EO_{96}PO_{39}EO_{96}$ for 9% and 20% copolymer concentrations. It appears that, when R_c is plotted against the reduced temperature T-T_{cm1}, the data follow a common master curve with the empiric scaling relation:

$$R_c \propto (T - T_{cm1})^{0.2} \tag{20}$$

Figure 11. The micellar core-radius of various PEO-PPO-PEO block copolymer micelles plotted versus the relative temperature $T - T_{cm1}$, T_{cm1} being the critical micellation temperature [34]. The scale on the left axis gives the aggregation number N.

The aggregation number N_{agg} can be calculated from the the core dimension. If we assume that the core consist only of propylene oxide, we have

$$4\pi R_c^3/3 = N_{agg} \cdot n \cdot V_{PO} \tag{21}$$

where n=40 is the poly(propylene oxide) degree of polymerization. V_{PO}=$M_{PO}/(\rho_{PO}N_A)$ is the dry propylene oxide volume. With the molar weight M_{PO}=58 and the mass density ρ_{PO}=1.01g/cm^3 we get V_{PO}=95.4Å^3 This leads to an aggregation number of $N_{agg} \approx 58$ at T=20°C and $N_{agg} \approx 116$ at T=40°C.

5.2.2. Critical Micellar Values and Micellar Volume Fraction

One of the important parameters obtained from fits to the experimental scattering function is the micellar volume fraction, ϕ.

In Fig. 13 and Fig. 12 are shown the micellar volume fraction of a 28% aquous solution of $EO_{96}PO_{39}EO_{96}$ (F88) as a function of respectively temperature and pressure. One see that at low temperatures, the micellar volume fraction is zero corresponding to that all copolymers is dissolved as independent unimers.

Above a well defined critical micellation temperature, T_{cm1}, there appear a broad range where micelles and unimers coexists thermodynamically. The micellar volume fraction increases roughly linearly with temperature and reaches an approximately constant level above a second characteristic temperature, T_{cm2}. Above T_{cm2} 'all' copolymers have aggregated in micelles. The broad range with linear increase in micelle density is rather different from low-molecular surfactants, which at the critical micellar temperature typically shows a step-like function in micelle-concentration. The origin of the broad range where significant concentrations of both micelles and unimers coexist may be a result of the polymeric nature, including polydispersity.

The application of hydrostatic pressure, Fig. 12 has an effect corresponding to lowering the temperature, i.e. PPO get more hydrophilic upon application of pressure.

For polymer concentrations below approximately 20%, the limiting micellar volume fraction, ϕ_o varies linearly with concentration [54,33]. This is in agreement with the

Figure 12. The micellar volume fraction of an aqueous solution of 28% $EO_{96}PO_{39}EO_{96}$ block copolymer, as obtained versus pressure [12].

Figure 13. The micellar volume fraction of an aqueous solution of 28% $EO_{96}PO_{39}EO_{96}$ block copolymer, as obtained versus temperature [19].

postulate that all polymers have aggregated in micelles above T_{cm2}. Above c ~20%, on the other hand, the micelle volume fraction reach a limit of the order of ϕ_c ~0.53. In this regime there therefore remain some unimers present. The ϕ=0.53 value is the critical value for hard-sphere crystal formation [43,19], and will be discuss further below.

The aggregation number, which was discussed above on the basis of the size of the micellar core, can be independently calculated on the basis of the micellar volume fraction. In the regime where ϕ increases linearly with temperature, the system is thermodynamic stable with both micelles and polymers present. The number of micelles per volume, ϕ/V_{hs}, (V_{hs}=$4\pi/3R_{hs}^3$ being the hard-sphere micelle volume) and the number of free chains per volume, n_p, is related through

$$n_p + N_{agg} \cdot \phi/V_{hs} = c/V_p \tag{22}$$

where c/V_p represents the total concentration of polymer chains, V_p being the dry volume of the polymer. Above T_{cm2} there are basically no free polymer chains, i.e. n_p=0. This leads to the aggregation number:

$$N_{agg} = c/\phi_o \cdot 4\pi R_{hs}^3/3V_p \tag{23}$$

where ϕ_o=$\phi_o(c)$ is the saturating value, linearly dependent on polymer-concentration c. The dry polymer volume is given as the sum of the volume of monomers, V_p=$2mV_{EO}$+nV_{PO},

where V_i=$M_i/(\rho_i N_A)$, i=PO or EO. V_{PO}=95.4Å^3 as given above, and with M_{EO}=44 and ρ_{EO}=1.01 g/cm^3 the ethylene oxide volume is V_{EO}=73.1Å^3. Using the fitted value for R_{hs} we then get an aggregation number of $N_{agg}\approx$37 at 20^{o}C, increasing to 78 at 40^{o}C for the $EO_{25}PO_{40}EO_{25}$ copolymer micelles. These values are slightly smaller than those obtained from the core-dimension. If we, on the other hand, use a more realistic model where the core dimensions are given by a dense propylene oxide core covered by a dense monolayer shell of ethylene oxide we get, within the whole temperature-regime, perfect agreement between the two routes of calculating the aggregation number. The effective thickness of the dense EO-shell is then 2.8Å.

Figure 14. Contour plot of the micellar volume fraction of the $EO_{25}PO_{40}EO_{25}$ system as a function of polymer concentration and temperature. The broken lines separates pure unimer phase (I), pure spherical micellar phase (III) and coexisting micellar and unimer phase (II). The solid line represents ϕ=0.53 and separates liquid and para-crystalline phase (IV).

In Fig. 14 is shown in a contour plot the micellar volume fraction as resulting from neutron scattering data of $EO_{25}PO_{40}EO_{25}$ obtained for polymer concentrations in the range 0-40% and at temperatures up to 50°C, i.e. the range of spherical micelles. The variation in ϕ separates into 4 regimes as indicated in the figure.

At low temperatures and concentrations (regime I in the figure), all polymers are dissolved as the unimers discussed above. Above a line of critical micellation temperatures (T_{cm1}) and concentrations (cmc_1), regime II, micelles and unimers coexists. The solution is totally dominated by micelles in regime III. The line separating phase II and III is well defined and reproducible characterized by the relative concentration independent temperature T_{cm2}.

For polymer concentrations below approximately 20%, the limiting micellar volume fraction, ϕ_o, varies linearly with concentration (phase-III), as discussed above. Above c ~20%, on the other hand, the micellar volume fraction reach a limit of the order of

ϕ_c ~0.53 (phase-IV). In this regime the micelles form an ordered structure, as discussed below.

For constant polymer concentration below 20%, Fig. 14 shows a minor decrease in micellar volume fraction in the high temperatures phase-III. This reflects the increasing aggregation number, resulting in larger micelles which occupy less volume.

5.3. Rod-like Micelles

At high temperatures, the scattering pattern of many PEO-PPO-PEO copolymer micelles changes in character. For low concentrations of $EO_{25}PO_{40}EO_{25}$, this appears at approximately 70°C. Above $T \approx 70°$ the low angle scattering intensity increases and in the low concentration regime the characteristic correlation peak totally disappears.

Fig. 15 shows the scattering function of 1% $EO_{25}PO_{40}EO_{25}$ obtained at 80°C. The solid line is a fit to cylinder with axes 50Å and length 500Å. There are systematic differences which can be associated with contribution to the scattering from the PEO-chains and possibly polydispersity or deviation from rod-like (worm-like) form.

Figure 15. The scattering pattern of $EO_{25}PO_{40}EO_{25}$ in the rod phase. The solid line represents scattering from a cylinder with radius 50Å and length 500Å.

The low-temperature spherical micelles have apparently within a small temperature regime transformed into rod- or worm-like micelles. Based on Fourier transform of the scattering function it was anticipated [33] that the micelles within a narrow temperature range continuously change from spherical via prolate ellipsoids to worm- or rod-like micelles. The scattering data would, however, also be consistent with coexistence of spherical and worm-like micelles within the given temperature regime. Such behavior has recently been observed in a study combining neutron scattering and cryo-electron microscopy measurements on the closely related aqueous system of PEO-PIB-PEO, where PIB is poly(isobutylene) [44].

In block copolymer micelles of higher PEO-content, the phase lines (unimer-to-micelle

and spherical-to-rod) are shifted. In $EO_{99}PO_{65}EO_{99}$ and $EO_{96}PO_{39}EO_{96}$, f.ex., the sphere-to-rod transition for low polymer concentrations only appear at $T\approx 95°C$ [41,34], whereas the $EO_{96}PO_{39}EO_{96}$ appear at approximately 90°. On increasing polymer concentration, the sphere-to-rod transition temperature is reduced.

The origin of the sphere-to-rod transition is attributed to the size of the spherical aggregates. As seen from the plot Fig. 11 the core-radius of the spherical micelles increases markedly with increasing temperature. Close to $T=70^oC$ for low concentration $EO_{25}PO_{40}EO_{25}$, the core-radius approach 50Å giving on average only 2.5Å per PO-monomers for those chains crossing the micelle-center. This can be accommodated in two ways. Either the PPO-blocks are highly stretched which entropically is very costly, or there is a large mixing of EO and PO inside the core with a resulting increase in chemical potential [33]. Linse has in a lattice model calculated the chemical potential [45] and thereby theoretically verified that the rod-like structure due to these properties are favored at elevated temperatures.

5.4. Disc-like Micelles

At high polymer concentrations, many aqueous systems of PEO-PPO-PEO block copolymers form assemblies of disc-like or lamellae structure. Individual micelles of disc like form have been proposed in block copolymers of low PEO-content, eg. $EO_6PO_{36}EO_6$ [35]. The reason for disc like shape is in these system obviously resulting from the optimum way to shield the large core of non-soluble PPO-blocks.

A quite different reason for disc-like micelles can be found in for example micelles of polyethylene, PE, in which the form is governed by polymer crystallization. Diblock copolymers of PE and poly(ethylene propylene), PEP, form in decane large disc-like micelles, in which the PE-blocks have crystallized into extended lamellar sheets [46]. The sheets are surrounded on both sides by PEP brushes.

6. Micellar Liquid Crystalline Phase

In the contour plot of the micellar volume fraction, ϕ, shown in Fig. 14, we see that ϕ saturates at a limiting value of the order of $\phi_c\approx 0.53$. When this ϕ_c boarder-line is crossed the micellar liquid undergoes a first order phase transition to a cubic crystal [19] which constitute a transparent, paste-like material with elastic shear modulus of the order of 10^4-10^5Pa [47,48]. The liquid and crystalline domains coexist in the range between $\phi_c=0.47$ and $\phi_c=0.53$ [12] (see also Fig. 13 and Fig. 12). These characteristics are in agreement with simple hard-sphere crystallization [43].

The polycrystalline paste-like powder-sample is easily aligned into one macroscopic monodomain crystal upon application of simple continuous or oscillatory shear. In spite of the fact that the individual micellar aggregates are dynamic in the sense that copolymers on a short time scale move from one micelle to another, the mono domain crystalline phase remains for more than weeks after the shear has been stopped.

While the shear thus have dramatic influence on the texture, it does not have marked effects on the phase behavior of the PEO-PPO-PEO systems. There has been no observations of any shear dependence in the cubic phase for shear rates up to 6000 sec^{-1}. This is different from observations on crystalline ordered PS-PI diblock copolymer micelles in decane [20]. In the BCC phase of these PS-PI micelles, Gast *et al.* observe at moder-

ate shear rates a continuous deformation of the lattice into a twin structure with sliding crystalline layers. At higher shear rates the crystalline long range order is lost, and an amorphous or liquid-like structure develops. In micellar networks of triblock copolymers of PS-PEB-PS, the order-disorder phase transition temperature changes significantly by shear rate [49], as has been seen in pure melts of both di-block [50] and tri-block copolymer melts [51].

6.1. Single Crystal Crystallography

The poly-crystalline phase of PEO-PPO-PEO micelles can effectively be oriented in both the static shear of a Couette cell and in the oscillatory shear of plan-parallel devices, as shown in Fig. 5 and Fig. 6, respectively. In fact, the sample is so easy to shear align that mounting the material between two parallel plates (eg. quartz or aluminum) and by hand just move one plate relative to the other, results in a well oriented single phase crystal with mosaicity typically of the order of 10°. Such shear-oriented crystals are free to be rotated, and are accordingly suitable for crystallographic studies in the neutron beam, and thereby index the observed Bragg-reflections. Fig. 16 shows an example of such studies performed on $EO_{96}PO_{39}EO_{96}$-micelles. The figure shows two two-dimensional scattering pattern, obtained with the beam along the shear gradient and when the sample is rotated 35° around the primary [110]-reflection, respectively. The scattering conclude body centered cubic lattice, bcc, as indicated by the associated Miller indexes.

Figure 16. Two-dimensional scattering pattern of $EO_{96}PO_{39}EO_{96}$-micelles in the cubic bcc phase. The scattering pattern are obtained with the shear axis horizontal and with shear gradient parallel to the beam (left) and the with the sample rotated by 35° around the vertical axis (right), respectively.

Most classical hard-sphere systems crystallize on face-centered cubic, fcc, lattice, rather than bcc. The reason for bcc-phase in many micellar system is related to the influence of the polymer-chains dispersed into the solvent, given rise to a softening of the interaction potential. Only in the limit of a thin corona, the micelles are true hard-sphere systems and should form a fcc solid. As the corona and thereby the length scale of the repulsion increases, the micellar system favors bcc symmetry. This has been nicely demonstrated experimentally in PS-PI diblock copolymer micelles [52].

Experiments on the cubic mesophase of PEO-PPO-PEO micelles have always revealed the shear gradient parallel to [111] and with the flow direction parallel to [112]. [110]-types of Bragg reflections dominates therefore the scattering pattern, as shown in the examples given in Fig. 17. In the two-phase regime with $0.47<\phi<0.53$, the orientation appears, however, to depend on both history and applied shear field. While the [111]-axis is still parallel to the shear gradient, both [112] and [110]-axes are found parallel to the flow direction.

Figure 17. Two-dimensional scattering pattern of ABA-type of block copolymer micelles: $EO_{25}PO_{40}EO_{25}$, $EO_{96}PO_{39}EO_{39}$, and $EO_{99}PO_{65}EO_{99}$; and BAB-type of block copolymer micelles: $PO_{15}EO_{165}PO_{15}$ in the cubic phases. The scattering pattern are obtained with the shear axis horizontal and shear gradient parallel to the beam.

In ordered phases of PPO-PEO-PPO triblock copolymer micellar networks, as discussed further below, equivalent shear orientation have been found in the cubic phase. In a triblock copolymer gel of polystyrene and poly(ethylene buthylene), PS-PEB-PS, on the other hand, the bcc cubic phase orient in a twinned structure arranged with a [111] direction parallel to the shear, and [100] direction parallel to the shear gradient, Fig. 18 [49]. This is the orientation typically observed in the ordered phase of amorphous

diblock copolymer melts (see eg. [53,13]) as well as classical systems like metals.

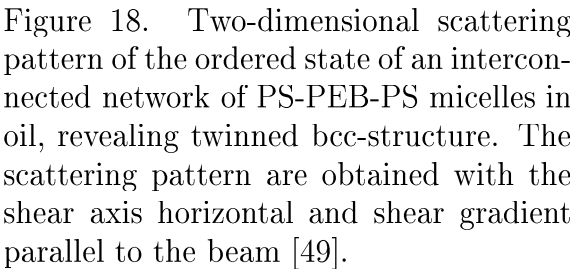

Figure 18. Two-dimensional scattering pattern of the ordered state of an interconnected network of PS-PEB-PS micelles in oil, revealing twinned bcc-structure. The scattering pattern are obtained with the shear axis horizontal and shear gradient parallel to the beam [49].

In the limit of high temperature and/or high polymer concentration, the cubic phase melts at the point where the spherical micelles transform into rod-like form, as discussed above. In some systems, eg. $EO_{25}PO_{40}EO_{25}$ [54], there are a separate phase between the cubic and the hexagonal rod-phase. Other materials, e.g. ($EO_{27}PO_{61}EO_{27}$) [55], shows a direct transition from the cubic to the hexagonal. The cubic phase of $EO_{25}PO_{40}EO_{25}$ remains to concentrations of the order of 45-50 % copolymers. At 45 % the cubic phase is observed from the lowest temperature measured (5°C) up to T=17°C. In the 50 % copolymer sample no six-fold por other atterns characteristic of the bcc phase are observed.

6.2. Cubatic Order

The Bragg reflections of the micellar crystals of typical PEO-PPO-PEO systems are far from resolution limited. Analysis, including instrumental resolution, shows that the lineshapes are Lorentzian rather than Gaussian [19]. The correlation length (ξ) as obtained from Lorentzian fits to the first order reflections

$$\frac{d\sigma(q)}{d\Omega} = \frac{I_\circ}{1 + [(q - q_\circ) * \xi]^2} + I_i \tag{24}$$

shows a small discontinuity at T_m, in agreement with the first order phase transition. In the ordered phase, however, the correlation length remains typically only of the order of a few hundred Å, i.e. the bond-length correlation is only a few lattice constants (roughly 2, 6 and 10 lattice constants for $EO_{25}PO_{40}EO_{25}$, $EO_{96}PO_{39}EO_{96}$, and $EO_{99}PO_{65}EO_{99}$, respectively). The orientational order, on the other hand, is macroscopic. This indicate *cubatic* classification of the crystalline state[19]. This para-crystalline nature markedly reduce the intensity of higher order reflections.

The reason for the cubatic nature of the ordered phase of PEO-PPO-PEO-micelles is unclear. It is possibly that the polydispersity in the micellar size play a role. Pluronics with large PEO-blocks tend to make more well characterized spherical micelles, as evident from the more pronounced side peaks in the form factor. Accordingly one should expect both more narrow peaks, and better resolved higher order reflections. This is consistent with experiments on different Pluronics. Fig. 17 shows the shear oriented scattering pattern of $EO_{25}PO_{40}EO_{25}$, $EO_{96}PO_{39}EO_{96}$, $EO_{99}PO_{65}EO_{99}$, and $PO_{15}EO_{156}PO_{15}$. Note that the latter is of the reverse architecture PPO-PEO-PPO, making a network of interconnected micelles. Another effect which however also affect the higher order reflections in the Pluronics series is the ratio between core size and inter-micellar distance. The low PEO-content polymers form relative larger cores. Their form factor will accordingly reduce the intensity of higher order reflections.

7. Nematic Phase

Upon application of steady shear, rod or worm-like micelles align to various degree depending on polymer concentration and shear-rate. In the rod-phase of 1% $EO_{25}PO_{40}EP_{25}$ copolymer solution, shear has only a relative small effect, possibly as a result of both relative small rods and because of the low viscosity, i.e. high relaxation rate. In samples of higher polymer concentration, on the other hand, shear has a marked effect as displayed in Fig. 19.

Figure 19. Two-dimensional scattering pattern of a 10% aqueous solutions of $EO_{25}PO_{40}EO_{25}$ in the rod-phase, as a function of external shear rate.

Fig. 19 shows the shear dependence of a 10% solution of $EO_{25}PO_{40}EP_{25}$ as obtained approximately in the middle of the rod-phase (T=76°C). Although the data still have to be finally analyzed, it is clear that the micelles align in the shear field, forming a nematic phase. The degree of alignment can be quantified by the ratio between scattered intensity

parallel and perpendicular to the shear. For shear-rates below approximately 1000/sec a near linear increase in this order parameter is observed. For higher shear-rates, the value saturates at a finite number.

The anisotropic scattering pattern relaxes instantaneously back to an azimuthally isotropic structure when the shear is stopped. In the neutron scattering experiment we observe isotropic scattering within the time resolution of a few seconds after the shear has been stopped.

Other systems of rod-like micelles have shown a hexagonal phase even at low concentrations [56,57]. This is not the case for low concentration Pluronics. In an experiment of 10% $EO_{25}PO_{40}EP_{25}$ where the Couette cell was displaced from a 'through center' to a tangential configuration, there were no sixfold pattern as characteristic of the hexagonal phase. In higher concentration, on the other hand, the PEO-PPO-PEO block copolymer rod-like micelles clearly form a permanent hexagonal rod-structure, as discussed below. The exact transition between nematic and hexagonal order has not been identified, but seems to be somewhere between 10 and 20 % copolymer concentration.

8. Hexagonal Rod-Phase

In aqueous systems of $EO_{25}PO_{40}EP_{25}$ and related Pluronics, the rod-like micellar phase form a solid high viscous suspension for polymer concentrations approaching 15-20%. This solid-like phase appear to be hexagonally ordered rod structure.

As in the cubic phase, this phase can be oriented by shear in a Couette cell, or between two parallel plates allowing crystallographic studies. In Fig. 20 is shown the pattern with the beam respectively parallel and perpendicular to the shear gradient. Two reflections clearly appear in the parallel configuration, while the perpendicular configuration shows the six fold pattern characteristic of the hexagonal rod-pattern, i.e. the beam parallel to the flow and to the rods. No other reflections were observed at any sample orientation.

The two patterns shown in Fig. 20 are to some extend not in agreement with each other. Rotating the sample 90° we should not expect to see the two strong 1st order reflections at q_o, but only higher-order terms like those at $\sqrt{3} \times q_o$ (which is however not visible in these samples). The reason for first order peaks in the $q_x - q_z$-plane is that the shear oriented sample always consists of two types of domains. This becomes evident from a detailed study of scattering pattern in three dimensions. The major part of the sample have the $(1\bar{1}0)$-axis parallel to the shear gradient, but a minor part of the sample is aligned with the (110)-axis parallel to the shear gradient. The (001) rod-axis is always parallel to the shear flow. In studies using the Couette cell for shear alignment, it is actually scattering from the minor part of the sample which dominates, since the major part have no first order peaks in this scattering plane and there is no higher order reflections. In the 90°-orientation displayed in Fig.14b, however, the major part of the sample dominates. Similar observation of two-domain structure from hexagonally ordered rods have also been done in block-copolymer mesophases [58].

9. Lamellar Phases

Aqueous solutions of typical PEO-PPO-PEO block copolymers form lamellar mesophases within wide ranges of the temperature-concentration phase diagram. In the $EO_{25}PO_{40}EO_{25}$-

Figure 20. Two-dimensional scattering pattern of a 27% aqueous solutions of $EO_{25}PO_{40}EO_{25}$ in the hexagonal rod-phase. Left: xz-plane; right: yz-plane, where the x-axis is parallel to the flow and the y-axis is parallel to the shear gradient.

system, the lamellar phase is observed over the 0-90°C temperature range [59], for polymer concentrations of the order of 50% or more. In aqueous systems the low-PEO content copolymer, $EO_6PO_{36}EO_6$-system, the lamellar phase is stable already at 10% polymer concentration [35]. The scattering function of the lamellar phase is dominated by a single correlation peak with only weak or no higher order reflections.

In Fig. 21 is shown an example of the scattering function of a typical lamellar phase: a narrow first order Bragg peak and a shoulder indicating the second order reflection. The data represent that of a 30% solution of $EO_6PO_{36}EO_6$ [35]. The low-q scattering is typical for swollen lamellaes with major in-plane fluctuations. The lamellar periodicity, d, increases linearly with polymer concentration as expected for ideal one-dimensional swelling

$$d = \delta/\phi \tag{25}$$

with bilayer thickness δ and polymer volume fraction ϕ.

The scattering pattern of the lamellar phase becomes usually anisotropic when the sample is exposed to shear. The result is a characteristic pattern with two symmetrical broad arcs [59]. Studies of shear alignment of block-copolymer lamellar phases have revealed that such materials typically orient into one of two kind of crystal orientations: either in *parallel lamellar* (lamellae parallel to xz plane) or in *perpendicular lamellar* (lamellae parallel to xy-plane of shear). In the lamellar phase of PEO-PPO-PEO aqueous solutions one find usually lamellar domains in all directions which have the lamellaes parallel to the direction of flow (x-axis).

Figure 21. Scattering function of 30% $EO_6PO_{36}EO_6$ aqueous solution in the lamellar L_α-phase and in the bi-continuous L_3-phase [35].

10. Bi-continuous phases

While bi-continuous microemulsions frequently appear in ternary phase diagrams of oil, water and low-molecular surfactants, there has only recently been observations of such phases in binary systems of block copolymers and solvent. The first observation was made in an aqueous solution of the low PEO-content PEO-PPO-PEO triblock copolymer, $EO_6PO_{36}EO_6$ previously mentioned [35]. In Fig. 21 are shown scattering functions of 30% $EO_6PO_{36}EO_6$ solutions in the lamellar L_α-phase described above, and in the bi-continuous L_3 sponge-phase with the characteristic scattering function as described by Teubner and Strey [60].

More recently, the microemulsion sponge phases have been observed in systems of ABA tri-block copolymers dissolved in A-homopolymers [61] and in a ternary systems of AB-diblock copolymer and A- and B-homopolymers [62]

11. Block Copolymer Micellar Networks

While the ABA-kind of block copolymers form individual micelles which interact through hard-sphere like repulsions, quite different behavior can be expected for BAB-kind of aggregates.

The PPO-PEO-PPO BAB-kind of copolymers associate also in spherical micelles. Since, however, the water soluble block is in the middle, aqueous solutions form opaque materials because of interconnected domain structures as schematically visualized in Fig. 2. In the scattering pattern such domains of micellar networks are characterized by a major low-angle scattering on top of the pattern observed for individual micelles. Such behavior is observed, for example, in the system, $PO_{15}EO_{156}PO_{15}$. Only for polymer concentrations above approximately 50%, the network constitutes the whole sample. Within this 'isotropic' phase, single domain cubic ordered mesophases have been observed in analogy with the ABA kind of micellar systems, as shown in Fig. 17 [9]. Other interconnected micellar systems expand the whole material even at only few percents of copolymers [63].

The BAB-micellar systems have potentially interesting elastic properties as a result of the network structure. One may imagine that very well defined networks can be designed

with controllable sizes of both the rubber-like middle blocks and the knots formed by the micellar cores. One may even be able to control the position of the knots since these can be organized on a crystalline lattice. The dynamics of the individual molecules within PEO-PPO kind of polymers are very fast, which makes the elastic properties of this particular network beyond the frequency range of practical interests.

In triblock copolymer systems of crystalline or glass forming polymers, permanent stable networks are possibly. Tri-block copolymers of polystyrene, PS, and rubber like materials like poly(ethylene propylene), PEP, form such stable networks when dissolved in oil [63]. Already with a few percent of such polymers in the oil, a permanent network of interconnected glassy PS spheres is formed throughout the sample, resulting in rubber-like elastic material. In some parts of the phase diagram, these materials form solid like ordered structures in analogy with the independent ABA-micelles (Fig. 18) [49].

Figure 22. Two-dimensional scattering function of micellar network of PS-PEP-PS triblock copolymers in oil, as obtained when stretched to various degree [64,65].

Stretching these materials gives rice to interesting structures, as shown in the contour plot of Fig. 22 [65]. The scattering pattern of samples stretched up to roughly 100% shows markedly enhanced scattering intensity in specific positions: *pseudo Bragg reflections* revealing stretching induced positional order of the PS-cores. At higher stretching ratios butterfly shaped patterns appear indicating inhomogeneity in the distribution of micellar cores and links [64].

12. Phase behavior of bulk block copolymers

Bulk block copolymers form also ordered mesophases, as revealed through intense studies during the last decade. The ordered phases includes bcc-structure of spherical micelles, hexagonal ordering of rod-like micelles and lamellar phases. Moreover, the tri-continuous cubic Ia3d-phase has been observed as well as complex modulated lamellar phases [66].

The pristine PEO-PPO-PEO materials form lamellar phases at low temperatures [59]. In opposition to the mesophases of both most block copolymers studied as well as the block copolymer solutions, where the self-assembling is controlled by the Flory-Huggins solubility parameter, the PEO-PPO-PEO lamellar phase is formed as a consequence of the crystallization of PEO.

In $EO_{25}PO_{40}EO_{25}$ the scattering momentum of the [10]-Bragg reflection is q_{10}=0.0272 Å^{-1}, giving a lamellar periodicity of $d=2\pi/q_{10}$=230 Å. To accomodate this large periodicity both the PEO and the PPO blocks have to be highly stretched.

At the melting point of PEO the block copolymer material undergoes an order-to-disorder transition. In the disordered phase there are still some composition fluctuations, but the Flory-Huggins interaction parameter characterizing the PEO-PPO-PEO system is relative small: $\chi = 0.092$. For the typical polymer sizes N studied, this χ-value is too small to accomodate the χN-value needed for ordering.

Other related PEO-block copolymer melts based on comparable molecular weights have significant larger Flory-Huggins interaction parameters. This is the case for poly(ethyl ethylene)-poly(ethylene oxide) (PEE-PEO) which show a variety of χ-driven mesophases above the PEO-melting temperature, and a conventional order-disorder transition at higher temperature [67].

13. Concluding Remarks

In the present review we have described the use of small-angle neutron scattering to study block copolymer micellar phases. The technique provide experimental values for size and form of the polymers as well as their aggregates. It gives information on aggregation number and aggregation thermodynamics. The scattering experiments also provide information on the interactions between polymeric aggregates. It gives detailes on positional correlations between these structures, including detailed information on ordered structures.

It is shown that the aqueous systems of PEO-PPO-PEO triblock copolymers is a very good model system for experimental thermodynamic studies on the block copolymer self-assembly, as the amphiphilic character can be varied continously by changing either temperature or pressure.

The information obtained from scattering experiments can be used directly in the design and optimization of new polymeric materials. Moreover, experimental scattering studies of complex polymer systems provides a challenge for exploring new physical phenomena.

REFERENCES

1. B. Chu, Langmuir 11 (1995) 414.
2. M. Almgren, W. Brown and S. Hvidt, Colloid Polym. Sci. 273 (1995) 2.
3. P. Alexandriris, V. Athanassiou and T.A. Hatton, Langmuir 11 (1995) 2442.
4. K. Mortensen, J. Phys. Conden. Matter 25 (1996) A103..
5. J. Yang and G. Wegner 1992 Macromolecules 25 (1992) 1786.
6. Y.-Z. Luo, C.V. Nikolas, D. Attwood, J.H. Collett, C. Price, C. Booth, B. Chu and Z.-K. Zhou J. Chem. Soc. Faraday Trans. 89 (1993) 539.

7. C. Tsitsilianis, G. Staikos, A. Dondos, P. Lutz and P. Rempp, Polymer 33 (1992) 3369.
8. B. Gao and J. Kops, Polym. Bulletin 34 (1995) 279.
9. K. Mortensen, W. Brown, E. Jørgensen, Macromolecules 27 (1994) 5654.
10. O. Glatter and O. Kratky, Small-Angle X-Ray Scattering, Academic Press, 1982.
11. P. Alexandridis, U. Olsson and B. Lindman Langmuir 12 (1996) 1419.
12. K. Mortensen, D. Schwahn and S. Janssen, Phys. Rev. Lett. 71 (1993) 1728.
13. K. Koppi, F. Bates, K. Almdal, and K. Mortensen J. Rheology, 38 (1994) 999.
14. G. Hadziioannou, A. Mathis, and A. Skoulios, Colloid Polym. Sci. 257 (1979) 136.
15. K. Almdal, K. Koppi, and F.S. Bates, Macromolecules 26 (1993) 4058.
16. F.S. Bates, K. Koppi, M. Tirell, K. Almdal and K. Mortensen Macromolecules 27 (1994) 5934.
17. B. Ackerson, J.B. Hayter, N. Clark and L. Cotter, J.Chem.Phys. 84 (1986) 2344.
18. se f.ex. H.M. Lang et al, J. Rheol. 36 (1992) 743.
19. K. Mortensen, W. Brown, and B. Nordén Phys.Rev.Lett. 68 (1992) 2340.
20. G.A. McConnell, M.Y. Lin and A. Gast, Macromolecules 28 (1995) 6754.
21. K, Mortensen, K. Almdal, F.S. Bates, K. Koppi, M. Tirell and B. Nordén, Physica B213 (1995) 682.
22. A. Guinier and G. Fournet, Small-Angle Scattering of X-Ray, J. Willey & Sons, 1955.
23. R. Hosemann and S. N. Bagchi, Direct Analysis of Diffraction by Matter, North-Holland, Amsterdam, 1962.
24. J.S. Higgins and H.C. Benoit, Polymers and Neutron Scattering, Oxford Science Publ., Oxford 1994.
25. J.S. Pedersen, J. Appl. Cryst. 27 (1994) 595.
26. M. Kotlarchyk and S.-H. Chen, J. Chem. Phys. 79 (1983) 2461.
27. B. Svensson, P. Alexandridis, U. Olsson and K. Mortensen, To be published (1997).
28. J.S. Pedersen, J. Colloid. Polymer Science. To be published (1997).
29. J.S. Pedersen and M. Gerstenberg, Macromolecules 29 (1996) 1363.
30. J.K. Percus and G.J. Yevick, Phys. Rev. 110 (1958) 1.
31. N.W. Ashcroft and J. Lekner, Phys. Rev. 145 (1966) 83.
32. D.J. Kinning and E.L. Thomas, Macromolecules 17 (1984) 1712.
33. K. Mortensen and J.S. Pedersen, Macromolecules 26 (1993) 805.
34. K. Mortensen and W. Brown, Macromolecules 26 (1993) 4128.
35. E. Hecht, K. Mortensen and H. Hoffmann, Macromolecules 28 (1995) 5465.
36. H. Rosch, *in Nonionic Surfactants*, Ed. M.J.Schick, Dekker, New York (1967).
37. Z. Zhou and B. Chu, J. Colloid. Interface Sci. 126 (1988) 171.
38. S.M. Aharoni, Macromolecules 16 (1983) 1722.
39. P. Linse, Macromolecules 26 (1993) 4437.
40. P. Alexandridis, J.F. Holzwarth and T.A. Hatton, Macromolecules 27 (1994) 2414.
41. K. Mortensen and Y. Talmon Macromolecules 28 (1995) 8829.
42. O. Glatter, G. Scherf, K. Shillen and W. Brown, Macromolecules 27 (1994) 6046.
43. M.O. Robbins, K. Kremer and G.S. Grest, J. Chem. Phys. 88 (1988) 3286.
44. K. Mortensen, Y. Talmon, B. Gao and J. Kops, To be published (1997).
45. P. Linse, J.Phys.Chem. 97 (1993) 13896.
46. D. Richter, D. Schneiders, M. Monkenbusch, L. Willner, L.J. Fetters, J.S. Huang, M.

Lin, K. Mortensen and B. Farago, Macromolecules, (1996) in press.
47. W. Brown, K. Schillen, M. Almgren, S. Hvidt and P. Bahadur, J. Phys. Chem. 95 (1991) 1850.
48. G. Wanka, H. Hoffmann and W. Ulbricht, Colloid Polym. Science 268 (1990) 101.
49. R. Kleppinger, K. Mortensen, N. Mischenko, K. Almdal and H. Reynaers To be published (1997).
50. K. Almdal, K. Mortensen, K. Koppi, M. Tirell and F.S. Bates, J. Physique II (France) 617 (1996).
51. T. Tepe D. Hajduk, M.A. Hillmyer, P.A. Weimann, M. Tirell, F.S. Bates, K. Almdal, and K. Mortensen, To be published (1997).
52. McConnell GA, Gast AP, Huang JS, and Smith DJ 1993 Phys. Rev. Lett. **71** 2102
53. K. Almdal, K.A. Koppi and F.S. Bates, Macromolecules 26 (1993) 4058.
54. Mortensen K 1992 Europhys. Lett. **19** 599
55. K. Mortensen, Unpublished.
56. W.A. Hamilton, P.D. Butler, S.M. Baker, G.S. Smith, J.B. Hayter, L.J. Magid and R. Pynn, Phys.Rev.Lett. 72 (1994) 2219.
57. W.A. Hamilton, P.D. Butler, S.M. Baker, G.S. Smith, J.B. Hayter, L.J. Magid and R. Pynn, Phys.Rev.Lett. 74 (1995) 335.
58. F.S. Bates, K.A. Koppi, M. Tirrell, K. Almdal and K Mortensen, Macromolecules 27 (1994) 5934.
59. K. Mortensen, W. Brown and E. Jørgensen, Macromolecules 28 (1995) 1458.
60. M. Teubner and R. Strey, J. Chem. Phys. 87 (1987) 3195.
61. J.H. Laurer, J.C. Fung, J.W. Sedat, D.A. Agard, S.D. Schmit, J. Samseth, K. Mortensen, R.J. Spontak, Langmuir, (1997) submitted.
62. F.S. Bates, W.W. Maurer, P.M. Lipic, M.A. Hillmyer, K. Almdal, K. Mortensen and T.P. Lodge To be published 1997.
63. N. Mischenko, K. Reynders, R. Scherrenberg, K. Mortensen, F. Fontaine, R. Graulus, and H. Reynaers, Macromolecules, 27 (1994) 2345.
64. K. Reynders, N. Mischenko, K. Mortensen, N. Overbergh and H. Reynaers, Macromolecules 28 (1995) 8699.
65. N. Mischenko, K. Reynders, K. Mortensen, and H. Reynaers. J. Polymer Science, Polymer Physics (1996)
66. F.S. Bates, M.F. Schultz, A.K. Khandpur, S. Förster, J.H. Rosedale, K. Almdal and K. Mortensen Trans. Faraday Soc. 98 (1994) 7.
67. M. Hillmyer, F.S. Bates, K. Almdal, K. Mortensen, and A. Ryan, Science 271 (1996) 976.